Inorganic Chemistry

Article

pubs.acs.org/IC

Solid State Complex Chemistry: Formation, Structure, and Properties of Homoleptic Tetracyanamidogermanates RbRE[Ge(CN$_2$)$_4$] (RE = La, Pr, Nd, Gd)

Markus Kalmutzki,[†] David Enseling,[‡] John E. C. Wren,[§] Scott Kroeker,[§] Victor V. Terskikh,[⊥] Thomas Jüstel,[‡] and H.-Jürgen Meyer*[,†]

[†]Section for Solid State and Theoretical Inorganic Chemistry, Institute of Inorganic Chemistry, Universität Tübingen, Auf der Morgenstelle 18, 72076 Tübingen, Germany

[‡]Department of Chemical Engineering, Münster University of Applied Sciences, Stegerwaldstraße 39, 48565 Steinfurt, Germany

[§]Department of Chemistry, University of Manitoba, Winnipeg, Manitoba R3T 2N2, Canada

[⊥]Measurement Science and Standards, National Research Council, Ottawa, Ontario, K1A 0R6, Canada

Supporting Information

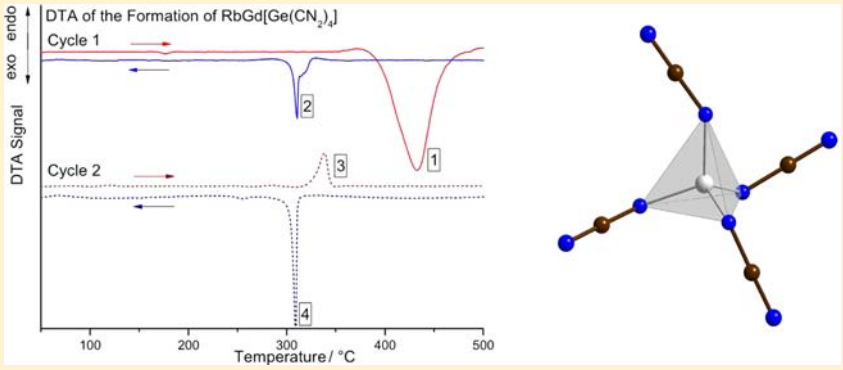

ABSTRACT: Tetracyanamidometallates with the general formula RbRE[T(CN$_2$)$_4$] (RE = La, Pr, Nd, Gd; T = Si, Ge) were prepared by solid state metathesis reactions starting from stoichiometric mixtures of RECl$_3$, A$_2$[TF$_6$], and Li$_2$(CN$_2$). Reactions were studied by differential thermal analysis that showed ignition temperatures between 360 and 390 °C for the formation of RbGd[T(CN$_2$)$_4$] with T = Si and Ge. The powder diffraction patterns of RbRE[Ge(CN$_2$)$_4$] were indexed isotypically to the already known RbRE[Si(CN$_2$)$_4$] compound. IR spectra of RbLa[Ge(CN$_2$)$_4$] were measured and compared with those of RbLa[Si(CN$_2$)$_4$]. ^{73}Ge, ^{87}Rb, and ^{139}La solid state NMR measurements and density functional theory calculations were used to verify the novel homoleptic [Ge(CN$_2$)$_4$]$^{4-}$ ion. Luminescence properties of Eu^{3+}, Ce^{3+}, and Tb^{3+} doped samples are reported.

INTRODUCTION

The chemistry of carbodiimides is a classic domain of organic and metal−organic chemistry, but an increasing number of cyanamide ([N—C≡N]$^{2-}$) or carbodiimide ([N═C═N]$^{2-}$) compounds that form essentially salt-like compounds with rare earth elements have been established over the past years.[1−6] Recently, complex [M(CN$_2$)$_4$]$^{n-}$ compounds with tetracyanamidosilicate (M = Si) and tetracyanamidoaluminate (M = Al) anions were prepared by solid state metathesis (SSM) reactions, and their crystal structures were determined and refined by X-ray diffraction (XRD) techniques.[4,5] Unique to these compounds are their homoleptic [M(CN$_2$)$_4$]$^{n-}$ ions, which can be considered as a sort of solid state coordination chemistry, paralleling compounds that are typically obtained from solution chemistry, however, with the absence of typical metal−organic ligands or solvent molecules. These compounds obtained from SSM reactions are usually insoluble in common solvents and may possess transport properties or other physical characteristics.[5]

A broader preparative development for this class of complex solid state compounds can be regarded for homoleptic or heteroleptic structures with [ML$_4$] or [ML$_6$] moieties with a main group element (M = group 13 or 14 element) as a central atom, and different ligand types (L = CN$_2^{2-}$, CN$^-$, OCN$^-$, ...) once appropriate conditions can be established for their preparation. Moreover, it will be of great interest to extend this chemistry to the preparation of compounds, where M is a transition metal, to parallel the chemistry of cyanometallates, which has been extensively developed by means of aqueous solution chemistry.[7]

Following our recent studies, we have extended our explorations toward the development of tetracyanamidometal-

Received: May 14, 2013
Published: October 24, 2013

lates following our original preparative strategy of SSM reactions. This type of reaction has been successfully used in the past for preparations of nitridoborates,[8] carbodiimides (cyanamides),[2,9] and cyanurates.[10] A remarkable advantage of solid state metathesis reactions for these families of compounds is that the respective anion can be transferred as a whole, as $[N{=}B{=}N]^{3-}$, $[N{=}C{=}N]^{2-}$, and $[O{=}C{=}N]^{-}$ from their alkali salts. This usually requires reactions with metal halides under moderate heating conditions (400−500 °C) following reactions 1 and 2. The largest variety of such compounds has been obtained by reactions with rare earth trihalides (REX_3 with X = F or Cl).[3,7,11]

$$3REX_3 + 3Li_3(BN_2) \rightarrow RE_3(B_3N_6) + 9LiX \quad (1)$$

$$2REX_3 + 3Li_2(CN_2) \rightarrow RE_2(CN_2)_3 + 6LiX \quad (2)$$

By the discovery of tetracyanamidosilicates, which were prepared by multilateral SSM reactions, the new family of homoleptic tetracyanamidometallate compounds has been brought to light (3).[4,5]

$$RECl_3 + A_2[SiF_6] + 4Li_2[CN_2] \rightarrow ARE[Si(CN_2)_4] + 2LiCl + 6LiF + ACl \quad (3)$$

Up to now, tetracyanamidosilicates include a large series of $ARE[Si(CN_2)_4]$ compounds (A = K, Rb, Cs; RE = Y, La−Lu). These compounds were recently complemented by the first examples of tetracyanamidoaluminates, $LiM_2[Al(CN_2)_4]$ with M = Sr, Eu,[12] as well as heteroleptic aluminates containing the $[Al(CN_2)_4(CN)F]^{7-}$ ion,[13] which were prepared by a corresponding way, starting from $A_3[AlF_6]$ or AlF_3.

Efforts to further expand this group of tetracyanamidometallate compounds have now led to the discovery of compounds containing the $[Ge(CN_2)_4]^{4-}$ anion with four examples being presented herein. Preparations of germanium(poly)-carbodiimides by means of solution metathesis routes were reported, but crystal structures remain unknown.[14] After the corresponding $ARE[Si(CN_2)_4]$ compounds doped with trivalent Ce, Eu, or Tb ions have shown interesting luminescence behavior, which was even reported to be significantly improved for the phase $EA_2[Si(CN_2)_{4-x}O_x]$:Eu (EA = alkali earth),[15] these properties are also studied for $RbRE[Ge(CN_2)_4]$ compounds and presented in this work.

EXPERIMENTAL SECTION

Synthesis. $Rb_2[GeF_6]$ was obtained after adding an appropriate amount of RbCl to a solution of H_2GeF_6, which was prepared by dissolving GeO_2 in hydrofluoric acid. After $Rb_2[GeF_6]$ precipitated, it was filtered off, washed several times with water, and dried at 150 °C in vacuum. The preparation of $Li_2(CN_2)$ has been reported previously.[3] The rare earth trichlorides ($RECl_3$) were prepared according to the literature.[16]

Manipulations of starting materials were performed in a glovebox under dry argon atmosphere. The starting materials $LaCl_3$, $Rb_2[GeF_6]$ (or $Rb_2[SiF_6]$), and $Li_2(CN_2)$ were mixed together in an agate mortar in a 1:1:4 molar ratio (total mass approximately 300 mg). Doped samples were prepared from mixtures of $LaCl_3$, $RECl_3$ (RE = Ce, Eu, Tb), $Rb_2[GeF_6]$ (or $Rb_2[SiF_6]$), and $Li_2(CN_2)$ in a 0.95:0.05:1:4 molar ratio. Each mixture was sealed into a silica ampule under vacuum, heated to 450 °C (550 °C) within 4 h, and remained at this temperature for 24 h (48 h) before being cooled to room temperature within 4 h. The silica ampule was opened in air, and the product was obtained as a crystalline powder. After products were rinsed with water several times and rinsing/drying with alcohol, they were inspected by XRD.

Thermal Analysis. Differential thermal analyses (DTA) were performed with a Netzsch Jupiter, STA 449 F3 apparatus between room temperature and 600 °C. Samples of the reaction partners were employed as described in the synthesis part with total masses of 100 mg and sealed into homemade silica tube sample holders ($V \approx 0.2$ cm^3) under an argon atmosphere.

X-ray Powder Diffraction. Reaction products were inspected by X-ray powder diffraction, recorded with a Stadi-P (STOE, Darmstadt) powder diffractometer, using germanium monochromated Cu $K\alpha_1$ radiation, and a Mythen 1 K detector. It could be shown that all preparations yielded similar XRD patterns for $RbRE[T(CN_2)_4]$ (RE = La, Pr, Nd, Gd; T = Si, Ge) plus the coproduced metathesis salts (LiF, LiCl, and RbCl) for unwashed samples. Washed samples contained sparingly soluble LiF, without any other detectable side-phase being present in the diffraction patterns.

Solid State NMR. ^{29}Si, ^{87}Rb, and ^{139}La spectra were collected on a Varian ^{UNITY}Inova 600 (14.1 T) NMR spectrometer in a 3.2 mm magic-angle spinning (MAS) probe. The NMR spectra were collected using single-pulse (i.e., Bloch-decay) excitation employing a 30° tip angle. ^{29}Si experiments used an optimized recycle delay of 120 s with up to 3000 coadded transients. ^{87}Rb and ^{139}La spectra were collected with optimized recycle delays of 2 s and 4000−12 000 coadded transients.

^{73}Ge, ^{87}Rb, and ^{139}La NMR spectra were collected on a Bruker Avance II 900 (21.1 T) spectrometer at the National Ultrahigh-field NMR Facility for Solids in Ottawa, Canada. MAS spectra were collected using solid-echo ($\pi/2 - \pi/2$) experiments in 7 mm, 4 mm, or 3.2 mm rotors at rotational frequencies of 5, 18, and 20 kHz, respectively. Optimized recycle delays were 2s (^{87}Rb, ^{139}La) and 10s (^{73}Ge). Spectra were collected with 5000−16 000 coadded transients. The time-domain spectra were "left-shifted" prior to Fourier transformation such that the first point was the most intense point of the echo signal.

^{29}Si spectra were referenced to the shift of hexamethyldisiloxane at +6.53 ppm with respect to TMS. ^{73}Ge spectra were referenced to germanium(IV) chloride as a secondary reference (+30.9 ppm) with respect to tetramethylgermanium. ^{87}Rb spectra were referenced with respect to 1 M $RbNO_3$(aq) and ^{139}La spectra with respect to 1 M $LaCl_3$(aq). Spectral modeling was done using the WSolids software package.[17]

Quantum Chemical Calculations. Density functional theory calculations (DFT) were performed using CASTEP,[18] a GIPAW (gauge-including projector augmented waves) computational method optimized for the calculation of electronic properties in periodic solids. Calculations implemented Perdew−Burke−Ernzerhof (PBE) functionals in the generalized gradient approximation (GGA) for the exchange-correlation energy and ultrasoft pseudopotentials. Fine-accuracy plane−wave basis sets with a 400 eV cutoff were used and relativistic effects were included using the scalar-relativistic zero-order regular approximation (ZORA). The Monkhorst-Pack grid had a maximum density of up to 3 × 3 × 3 *k*-points. The CASTEP code was run in the Materials Studio 4.4 environment on an HP xw4400 workstation with a single Intel Dual-Core 2.67 GHz processor and 8 GB DDR RAM. Calculated magnetic shieldings were converted to chemical shifts using CASTEP calculations of convenient reference compounds (^{29}Si, $Si(CH_3)_4$; ^{73}Ge, $Ge(CH_3)_4$) or previously established absolute shielding constants.[19]

The structural models for these calculations are based on the published crystal structure of $RbLa[Si(CN_2)_4]$.[4] Calculations on $RbLa[Ge(CN_2)_4]$ used the elemental positions of the $RbLa[Si(CN_2)_4]$ structure, except with Ge substituted for Si, and the experimental $RbLa[Ge(CN_2)_4]$ unit cell parameters measured by powder X-ray diffraction. Geometry optimization within these constraints yielded the final $RbLa[Ge(CN_2)_4]$ structure from which NMR parameters were calculated.

Infrared Spectra. Vibrational spectra were recorded with a Bruker Tensor 27 FT-IR spectrometer within the range of 400−4000 cm^{-1} by using KBr pellets.

Luminescence Spectroscopy. Excitation and emission spectra were collected with a fluorescence spectrometer FLS920 (Edinburgh

dx.doi.org/10.1021/ic401201w | *Inorg. Chem.* 2013, 52, 12372−12382

Instruments) equipped with a 450 W ozone-free xenon arc lamp (OSRAM) and a sample chamber installed with a mirror optic for powder samples. For detection, a R2658P single-photon counting photomultiplier tube (Hamamatsu) was used. All luminescence spectra were recorded in triplicate with a spectral resolution of 1 nm, a dwell time of 0.4 s in 1 nm steps. Reflection spectra were monitored by placing the sample into an integrating sphere coated with barium sulfate and using a synchronic scan (i.e., the excitation and emission monochromator were adjusted to the same wavelength and tuned synchronously). These reflection spectra were recorded on Edinburgh Instruments FS900 spectrometer equipped with a 450 W Xe arc lamp and cooled single-photon counting photomultiplier (Hamamatsu R928). $BaSO_4$ (99%, Sigma-Aldrich) was used as a reflectance standard.

RESULTS AND DISCUSSION

Synthesis and DTA. The new $RbRE[Ge(CN_2)_4]$ compounds were prepared by SSM reactions from mixtures of $Rb[GeF_6]$, $RECl_3$, and $Li_2(CN_2)$ in fused silica tubes according to reaction 4. The course of the reaction was controlled by differential thermal analyses (DTA) starting from a typical reaction mixture described in the synthesis part, which was fused into a homemade silica tube sample holder.

$$RECl_3 + Rb_2[GeF_6] + 4Li_2(CN_2) \rightarrow RbRE[Ge(CN_2)_4] + 2LiCl + 6LiF + 1RbCl \quad (4)$$

The thermoanalytical study (via DTA) of the formation of $RbGd[Ge(CN_2)_4]$ was compared with that of $RbGd[Si(CN_2)_4]$ to get a deeper understanding of this type of reactions. The formation reaction of $RbGd[Si(CN_2)_4]$ given in eq 3 is regarded to correspond to the reaction given in eq 4.

DTA experiments were performed by two heating and cooling cycles, as displayed in Figures 1 and 2. The first cycle for the preparation of $RbGd[Ge(CN_2)_4]$ (Figure 1) shows two major thermal effects: an exothermic effect due to the formation of the product on heating (centered at 432 °C, marked as 1) and an endothermic effect due to crystallization (peak at 310 °C, marked as 2) when the mixture is cooled to room temperature. The crystallization temperature is close to the melting point of the eutectic LiCl–RbCl mixture (312 °C).[20] The second cycle shows an endothermic effect (304 °C, marked as 3) due to the melting of the flux on heating, and an exothermic effect (309 °C, marked as 4) due to its crystallization. A similar behavior is obtained in the DTA of $RbGd[Si(CN_2)_4]$ (Figure 2) with an exothermic formation on heating, and a recrystallization effect on cooling. Again, the second cycle represents the melting and recrystallization of the in situ generated flux.

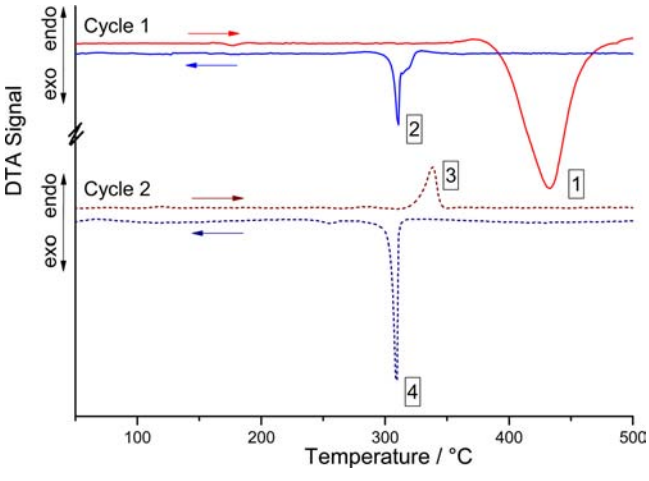

Figure 1. DTA between room temperature and 500 °C (heating and cooling rate of 2 K/min.) starting from a reaction mixture of $Rb_2[GeF_6]$, $GdCl_3$, and $Li_2(CN_2)$ with the formation of $RbGd[Ge(CN_2)_4]$, LiF, LiCl, and RbCl. Cycle 1: Melting of the in situ generated flux and formation of $RbGd[Ge(CN_2)_4]$ (**1**, centered at 432 °C) on heating, and recrystallization (**2**, 310 °C) on cooling. Cycle 2: DTA starting from the mixture formed after cycle 1, showing the melting of the flux mixture (**3**, 339 °C) on heating and recrystallization (**4**, 309 °C) on cooling.

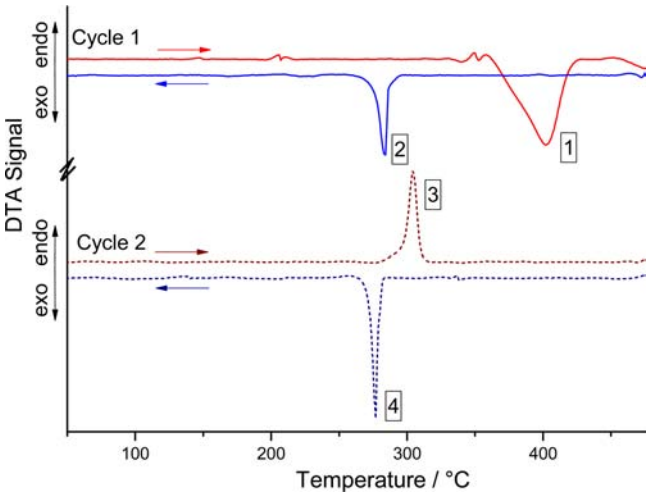

Figure 2. DTA between room temperature and 475 °C (heating and cooling rate of 2 K/min.) starting from a reaction mixture of $Rb_2[SiF_6]$, $GdCl_3$, and $Li_2(CN_2)$ with the formation of $RbGd[Si(CN_2)_4]$, LiF, LiCl, and RbCl. Cycle 1: Melting of the in situ generated flux and formation of $RbGd[Si(CN_2)_4]$ (**1**, centered at 402 °C) on heating, and recrystallization (**2**, 284 °C) on cooling. Cycle 2: DTA starting from the mixture formed after cycle 1, showing the melting of the flux mixture (**3**, 304 °C) on heating and recrystallization (**4**, 277 °C) on cooling.

From these investigations it is clear that both reactions are perfect examples of solid state metathesis reactions. Upon heating, the reaction is ignited at rather low temperatures ($T_i \approx$ 390 °C for $RbGd[Ge(CN_2)_4]$ and $T_i \approx$ 360 °C for $RbGd[Si(CN_2)_4]$) and is promoted by its own heat generation. During the reaction, a flux system is created, causing a melting process in the reaction mixture, thus improving the diffusion and in turn speeding up the reaction. All these effects are responsible for rather short reaction times, low reaction temperatures, and complete conversion rates of reactions. We noted that both systems require quite similar heating programs and temperatures for the $RbRE[T(CN_2)_4]$ synthesis. However, no single crystals were obtained in reactions with germanates, only microcrystalline powders. Crystalline powders of $RbRE[T(CN_2)_4]$ appear to behave stable in air and in water.

XRD and Crystal Structure. The materials synthesized according to reactions 3 and 4 were analyzed by XRD powder analyses and refinements. The washed samples show X-ray reflections only of the respective product and the metathesis salt (LiF) as displayed for $RbGd[T(CN_2)_4]$ for T = Si and Ge as shown in Figures 3 and 4. The powder patterns of $RbRE[Ge(CN_2)_4]$ compounds were indexed isotypically to the refined crystal structure of $RbLa[Si(CN_2)_4]$ with the space group $I\bar{4}$ and Z = 2. Lattice parameter refinements of

dx.doi.org/10.1021/ic401201w | Inorg. Chem. 2013, 52, 12372–12382

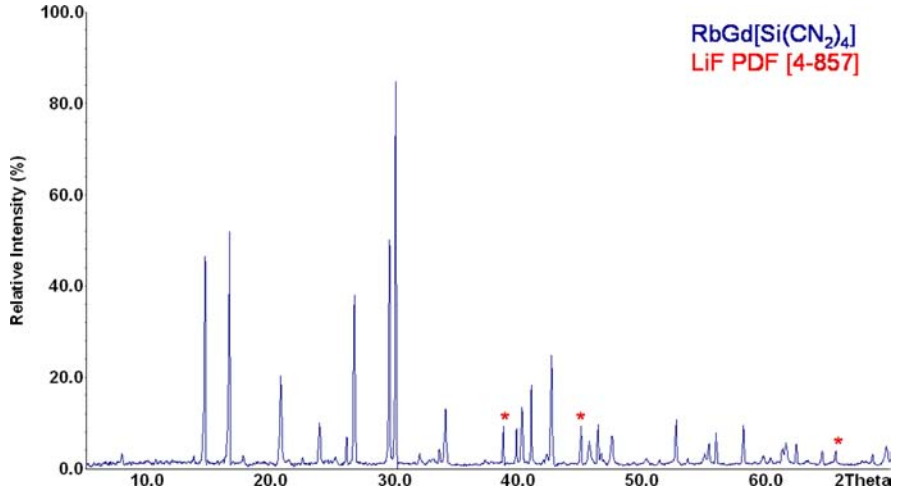

Figure 3. Recorded XRD powder pattern of RbGd[Si$(CN_2)_4$] and reflections corresponding to LiF [4−857] (stars).

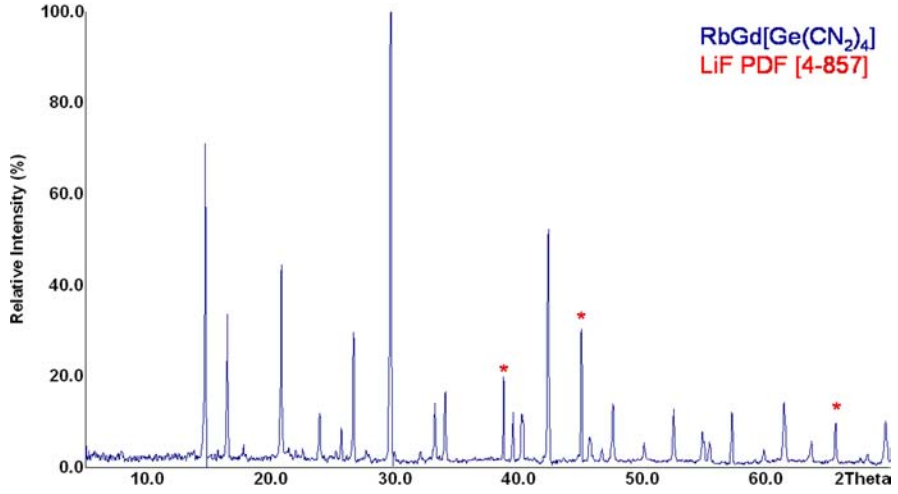

Figure 4. Recorded XRD powder pattern of RbGd[Ge$(CN_2)_4$] and reflections corresponding to LiF [4−857] (stars).

Table 1. Lattice Parameters (in Å) and Unit Cell Volumes (in Å^3) for RbRE[Ge$(CN_2)_4$] Compounds with Tetragonal Indexing

	RbLa[Ge$(CN_2)_4$]	RbPr[Ge$(CN_2)_4$]	RbNd[Ge$(CN_2)_4$]	RbGd[Ge$(CN_2)_4$]
a	8.5493(2)	8.462(2)	8.4556(1)	8.4075(2)
c	6.9557(2)	6.851(2)	6.8317(9)	6.7599(9)
V	507.7(3)	490.6(3)	488.4(2)	477.83(1)

RbRE[Ge$(CN_2)_4$] compounds were performed with the program WinXPOW[21] with the results displayed in Table 1.

The small differences of lattice parameters and of the resulting unit cell volumes between the isotypic RbGd[T-$(CN_2)_4$] compounds for T = Si and Ge (Δ = 7.93 Å^3 for Z = 2, equal to 3.965 Å^3 per tetrel) is in agreement with the volume difference (Δ = 5.45 Å^3 per tetrel) obtained between Si_3N_4 ($P6_3$, Z = 2, V = 144.99 Å^3, d_{Si-N} = 1.7044−1.7665 Å)[22] and Ge_3N_4 ($P6_3$, Z = 2, V = 171.75 Å^3, d_{Ge-N} = 1.8271−1.8495 Å).[23]

The atomic arrangement in the isotypic structures of RbRE[$T(CN_2)_4$] can be briefly described as follows: The rare earth and the tetrel element can be thought to form a NaCl-type arrangement, in which half of the tetrahedral holes are occupied by alkali metal ions. The tetrel element is coordinated by four almost linear $[NCN]^{2-}$ groups forming an almost regular TN_4 tetrahedron with bent T—N—C angles (Figure 5). The alternating distances in the cyanamide ion of the T—N—C≡N arrangement clearly tends toward values obtained in cyanamide (H_2N—C≡N: d(H)N—C(N) = 1.315 Å and d(HN)C≡N = 1.152 Å), as noted for the $[Si(NCN)_4]^{4-}$ ion.

The 8-fold coordination of the rare earth ions in the RbRE[T$(CN_2)_4$] (T = Ge, Si) structure is similar to that found for the rare earth ion in the garnet structure (e.g., $Y_3Al_5O_{12}$).

Solid State NMR. Lacking structural confirmation by single-crystal diffraction, we used solid state NMR to gain insight about the structure of RbLa[Ge$(CN_2)_4$]. ^{73}Ge is a challenging nucleus to probe by NMR due to its low resonance frequency, large quadrupole moment, and relatively low natural abundance.[24] For all of these reasons, NMR observation at high magnetic fields is advantageous. Figure 6b shows the ^{73}Ge MAS NMR spectrum of RbLa[Ge$(CN_2)_4$] collected at 21.1 T (900 MHz ^{1}H frequency) along with a single-site line shape simulation based on the following parameters: δ_{iso} = 29 ppm,

dx.doi.org/10.1021/ic401201w | Inorg. Chem. 2013, 52, 12372−12382

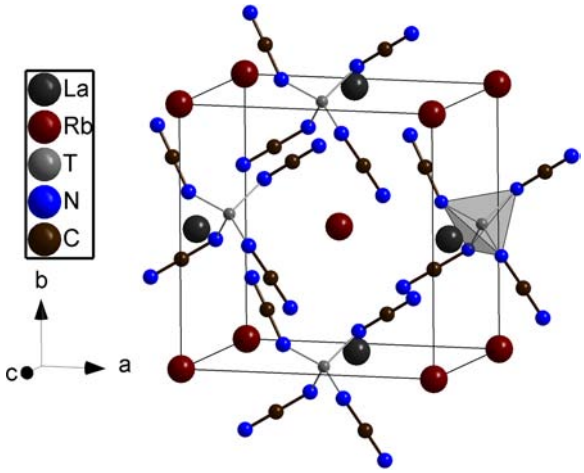

Figure 5. Projection of the tetragonal unit cell of $RbLa[T(CN_2)_4]$ (T = Si, Ge).

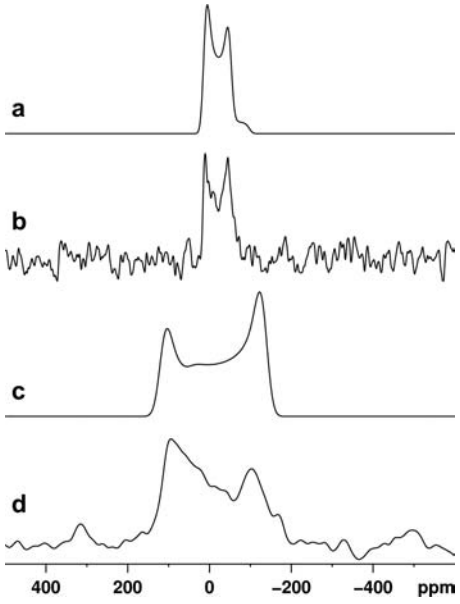

Figure 6. ^{73}Ge NMR spectra of solid $RbLa[Ge(CN_2)_4]$ at 21.1 T. (a) Simulated and (b) experimental MAS NMR spectra; (c) simulated and (d) experimental NMR spectra of a nonspinning sample. Simulation parameters are reported in Table 2.

C_Q = 6.0 MHz, and η = 0 (Figure 6a, Table 2). Although the isotropic chemical shift provides little structural information because there are so few ^{73}Ge NMR data with which to compare it, the quadrupolar coupling constant, C_Q, and quadrupolar asymmetry parameter, η, are more informative. C_Q, a direct measure of the largest component of the electric field gradient tensor at the nucleus, is sensitive to local symmetry such that high point-group symmetry yields values close to zero,[25] whereas more distorted sites can have C_Q values over 60 MHz.[24,26] The present value is considerably smaller than that of any of the germanates previously measured and closer to the values found for highly symmetrical tetrahedral organogermanes,[27] providing strong evidence that the local site symmetry is very high.

Additional support for a high degree of symmetry is the quadrupolar asymmetry parameter, η, which indicates axial symmetry at Ge. DFT calculations of C_Q were done using the $RbLa[Si(CN_2)_4]$ crystal structure with Ge in place of Si and the experimentally determined lattice parameters for $RbLa[Ge(CN_2)_4]$. The predicted C_Q is even smaller than that observed experimentally (Table 2). Although CASTEP is known to underestimate Ge C_Q's by 10−15%,[24] these calculations indicate that the electric field gradient at Ge should be very small in this structure.

To verify that the observed ^{73}Ge NMR spectrum arises from a single crystallographic site with a nonzero C_Q, and not two cubic sites, we collected the ^{73}Ge NMR spectrum of a nonspinning sample (Figure 6d). The resulting spectrum is clearly incompatible with the presence of two Ge sites at the MAS positions, confirming that the resonance arises from a single Ge site. Despite the relatively high symmetry at the central atom, the simulation of this spectrum required the inclusion of 30 ppm of anisotropic chemical shielding. DFT calculations predict the presence of appreciable shielding anisotropy, and the measured value is quantitatively consistent with earlier observations in organogermanes.[26] Although the fit is not perfect, the breadth of the experimental signal and the location of the main line shape features can only be reproduced with the reported values. Taken together, these experimental and theoretical NMR data provide strong support for a highly symmetrical Ge environment in $RbLa[Ge(CN_2)_4]$, which is likely isostructural with $RbLa[Si(CN_2)_4]$.

Another strategy for evaluating whether the crystal structure of $RbLa[Ge(CN_2)_4]$ is isostructural with that of $RbLa[Si(CN_2)_4]$ is to compare the NMR parameters of each compound. The experimentally determined parameters may also be compared with those calculated on the basis of the known structure for the Si compound.[4] Figures 7 and 8 compare the ^{87}Rb and ^{139}La MAS and nonspinning NMR spectra of both compounds at 21.1 T, along with their corresponding spectral fits. It is clear from these direct comparisons that the compounds possess remarkably similar spectral properties. The measured NMR parameters, confirmed by analysis at 14.1 T (Figures S1 and S2, Supporting Information), are reported in Table 2 and reveal close correspondence for δ_{iso}, C_Q, η, and Ω (note that CASTEP-calculated values of κ, α, β, and γ were used in the spectral simulations). The fact that they do not agree exactly is presumably due to geometrical effects from the different sizes of Ge and Si and subtle electronic differences between these central metals. The similarities among their C_Q values are especially noteworthy in view of the high sensitivity of their respective quadrupolar interactions to local electronic environments and geometry: ^{87}Rb C_Q's range from 0 in the rock−salt structure halides[28] to over 15 MHz in a typical rubidium borate,[29] whereas ^{139}La C_Q's exceeding 100 MHz have been measured in metallocenes.[30] Both ^{87}Rb and ^{139}La possess large quadrupole moments, which make their C_Q's very sensitive to local structure.[31] The axial quadrupolar symmetry observed in both compounds is consistent with the space group.

Not only are the experimental NMR parameters of the two compounds very similar, but they are also consistent with those calculated by GIPAW based on the same structural model (Table 2). Taking the $RbLa[Si(CN_2)_4]$ calculations as a benchmark for what level of agreement can be expected, it is apparent that the ^{87}Rb C_Q's and chemical shielding spans, Ω, are in good agreement, considering the range of possible values for these parameters.

The ^{139}La shielding anisotropies are slightly less well reproduced by the calculations, differing by up to 44 ppm

dx.doi.org/10.1021/ic401201w | Inorg. Chem. 2013, 52, 12372−12382

Table 2. Experimental and Theoretical NMR Parameters for RbLa[T(CN$_2$)$_4$] (T = Si, Ge)

		δ_{iso} (ppm)[a]	C_Q (MHz)[a,b]	η[a]	Ω (ppm)[a]	κ[c]	α[c]	β[c]	γ[c]
				RbLa[Si(CN$_2$)$_4$]					
^{29}Si	expt	−50 ± 2			n.d.				
	calc	−56			47	−1			
^{87}Rb	expt	−66 ± 1	5.4 ± 0.2	0.0	60 ± 5				
	calc	−63	4.9	0.0	73	1	0	0	0
^{139}La	expt	310 ± 1	2.5[e] ± 0.2	0.0	195 ± 5				
	calc	292	10.8	0.0	162	−1	90	90	180
				RbLa[Ge(CN$_2$)$_4$]					
^{73}Ge	expt	29 ± 1	6.0 ± 0.3	0.0	30 ± 5				
	calc	−53	−1.3	0.0	130	−1	90	90	180
^{87}Rb	expt	−55 ± 1	6.1 ± 0.2	0.0	50 ± 5				
	calc	−99	5.1	0.0	42	1	0	0	0
^{139}La	expt	330 ± 1	4.4 ± 0.2	0.0	170 ± 5				
	calc	322	21.7	0.0	126	−1	90	90	180

[a]Best fit parameters from MAS and nonspinning NMR data collected at 14.1 and 21.1 T. [b]Note that only absolute values of C_Q are measured experimentally. [c]Values calculated by GIPAW and used for spectral fitting of experimental spectra. [d]n.d. (not determined). [e]Determined from the breadth of the satellite transition spinning-sideband manifold.

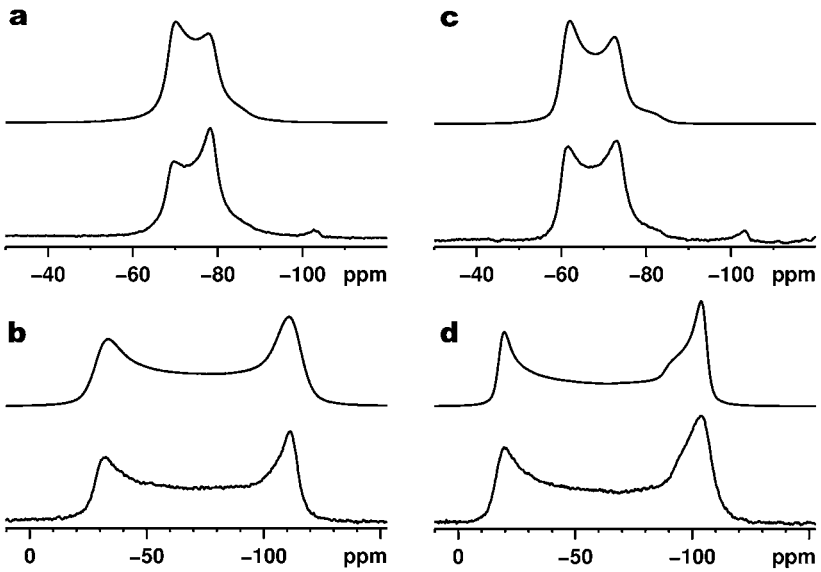

Figure 7. ^{87}Rb experimental (bottom traces) and calculated (top traces) NMR spectra at 21.1 T. (a) MAS and (b) nonspinning spectra of RbLa[Si(CN$_2$)$_4$]; (c) MAS and (d) nonspinning spectra of RbLa[Ge(CN$_2$)$_4$]. Simulation parameters are reported in Table 2.

from the experimental values. However, they are much closer than in recent work using comparable methodology, where the measured shielding span of 255 ppm in $LaNbO_4$ was calculated to be 490 ppm.[32]

For the ^{139}La C_Q in RbLa[Si(CN$_2$)$_4$], the calculations predict a significantly larger magnitude than is observed for both compounds; however, given the extremely high sensitivity of the quadrupolar interaction to local geometry, these calculations are not unreasonable. To probe the sensitivity of this parameter to structural effects, we calculated C_Q(^{139}La) for RbLa[Si(CN$_2$)$_4$] with small adjustments to the lattice parameters. Although C_Q(^{87}Rb) remains essentially invariant to modifications of *a* and *c*, C_Q(^{139}La) changes significantly. For example, a 1.5% increase in *a* brings C_Q(^{139}La) to 2.0 MHz, in near agreement with the experimentally measured value of 2.5 MHz. Whereas any elongation of the *c* axis increases C_Q(^{139}La), a 1.5% decrease in *c* reduces the original calculated value to 4.2 MHz. The measured C_Q(^{139}La) can be reproduced using lattice parameters of *a* = 8.642 Å and *c* = 6.818 Å, which represent a 1% increase in *a* and a 0.5% decrease in *c* relative to those determined by XRD. Although changes of 0.5−1.5% in the lattice parameters exceed the uncertainties reported in Table 1, these computational results illustrate the high sensitivity of solid state ^{139}La NMR and will further aid in the Rietveld refinement of the RbLa[Ge(CN$_2$)$_4$] crystal structure. Perhaps of even greater importance is the anisotropic response of ^{139}La NMR parameters to the crystal structure changes along the crystallographic directions, a matter of potential interest in studying thermal expansion properties in these materials.

In general, it may be noted that the calculations consistently predict the correct ordering of the NMR parameters for the two compounds. For example, the calculated and experimental ^{87}Rb and ^{139}La C_Q's are larger for RbLa[Ge(CN$_2$)$_4$] than for RbLa[Si(CN$_2$)$_4$] by about the same ratio. Conversely, the calculated and experimental ^{87}Rb and ^{139}La Ω values are uniformly smaller for RbLa[Ge(CN$_2$)$_4$] than for RbLa[Si(CN$_2$)$_4$]. Overall, the congruence of the experimental values

dx.doi.org/10.1021/ic401201w | Inorg. Chem. 2013, 52, 12372−12382

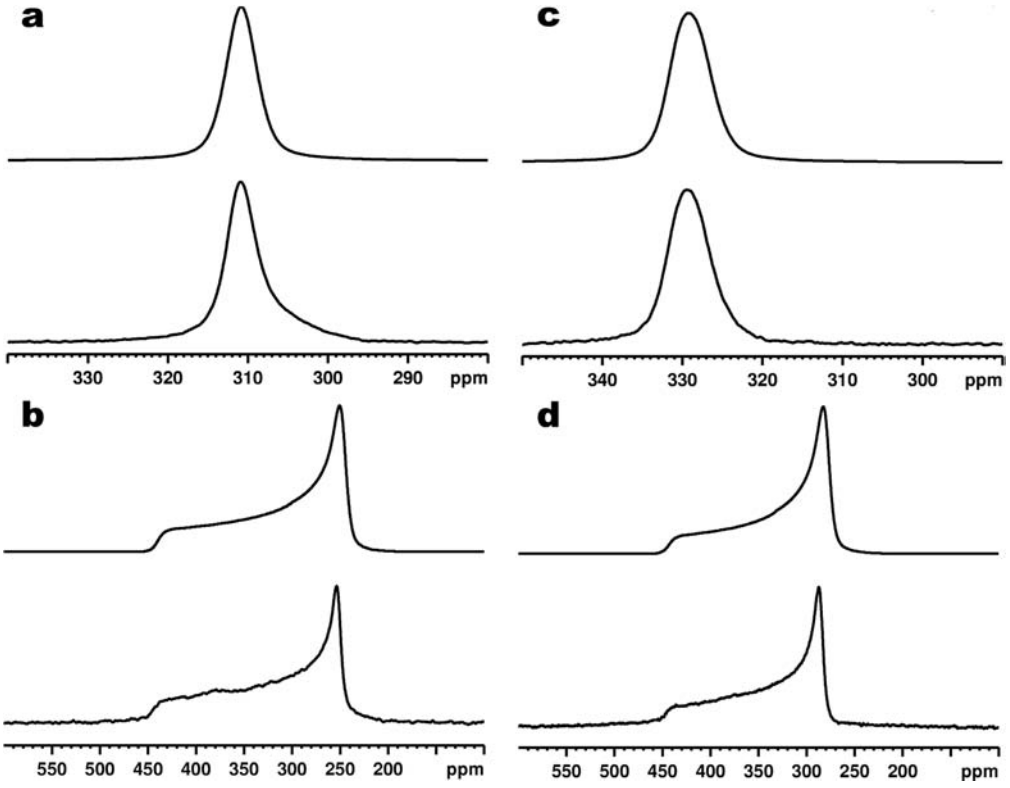

Figure 8. ^{139}La experimental (bottom traces) and calculated (top traces) NMR spectra at 21.1 T. (a) MAS and (b) nonspinning spectra of RbLa[Si(CN$_2$)$_4$]; (c) MAS and (d) nonspinning spectra of RbLa[Ge(CN$_2$)$_4$]. Simulation parameters are reported in Table 2.

with those calculated on the basis of the putative structure supports the structural conclusions.

For completeness, ^{29}Si MAS NMR was run on RbLa[Si(CN$_2$)$_4$] (Figure S3). A single silicon site was detected at δ_{iso} = −50 ± 2 ppm, in agreement with the shift previously observed for a tetrahedral SiN$_4$ environment.[33] The peak width of 440 Hz can be attributed to direct dipolar and indirect spin−spin coupling with bonded ^{14}N nuclei. The fact that these couplings are unresolved and contribute only to peak broadening is related to the quadrupolar nature of ^{14}N, which results in distorted multiplets not averaged by MAS.[34]

Luminescence and Reflection Spectroscopy. To determine the band gap of RbGd[Si(CN$_2$)$_4$] and RbGd[Ge(CN$_2$)$_4$], undoped single-phase samples were investigated by reflection spectroscopy (Figure 9). Both reflection spectra show a distinct absorption edge at about 380 nm (3.26 eV), which we interpret as the band gap. We assume that the upper edge of the valence band is composed by the occupied π-orbitals of the CN_2^{2-} groups (HOMO), whereas the lower edge of the conduction band is due to the empty 4s and 4p orbitals of Ge^{4+}. Therefore, the absorption process above 380 nm can be interpreted as a ligand to metal charge transfer, more precisely an electron transfer from $(NCN)^{2-}$ to Ge^{4+}.

Therefore, the blue emission band at 460−465 nm, which is observed for both compounds, is assigned as CT-luminescence. The large width of the emission band and the large Stokes Shift is typical for this kind of luminescence process.[35] Accordingly, the respective excitation band is located at about 370 nm, which corresponds to a Stokes shift of about 4400 cm^{-1} (Figures 10 and 11).

Figures 12 and 13 display the luminescence and reflection spectra of both compounds doped with Eu^{3+}. The emission spectra of RbGd[Si(CN$_2$)$_4$]:Eu^{3+} and RbGd[Ge(CN$_2$)$_4$]:Eu^{3+}

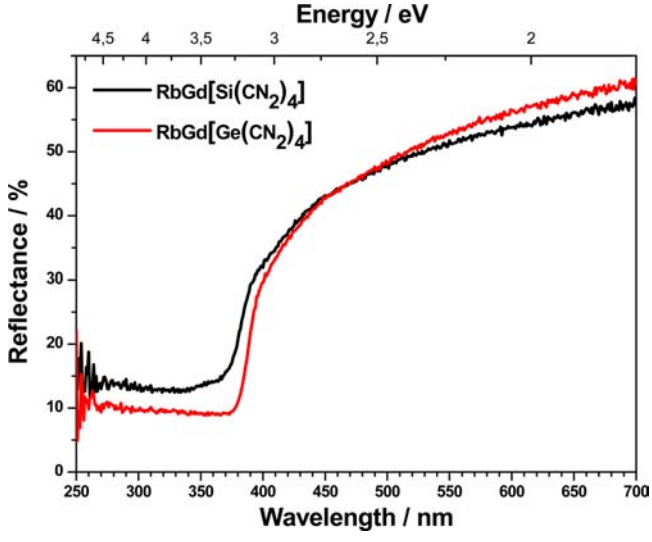

Figure 9. Reflection spectrum of a RbGd[Si(CN$_2$)$_4$] (black line) and RbGd[Ge(CN$_2$)$_4$] (red line) sample against BaSO$_4$ as a white standard.

upon 375 nm excitation are typical for Eu^{3+} doped luminescent materials and are thus governed by the $^5D_0 \rightarrow {}^7F_J$ transitions. Emission lines due to transitions from higher excited levels (e.g., $^5D_1$ or $^5D_2$) are not visible due to multiphonon quenching caused by the presence of high energy phonons (asymmetric vibration mode of CN_2^{2-} unit). The strongest emission lines, which are located at 611 and 617 nm, respectively, are attributed to the $^5D_0 \rightarrow {}^7F_2$ transitions. The intensity of lines originating from $^5D_0 \rightarrow {}^7F_1$ (≈596 nm) and $^5D_0 \rightarrow {}^7F_3$ (≈644 nm) are much weaker if compared to $^5D_0 \rightarrow {}^7F_2$ transition. The

dx.doi.org/10.1021/ic401201w | Inorg. Chem. 2013, 52, 12372−12382

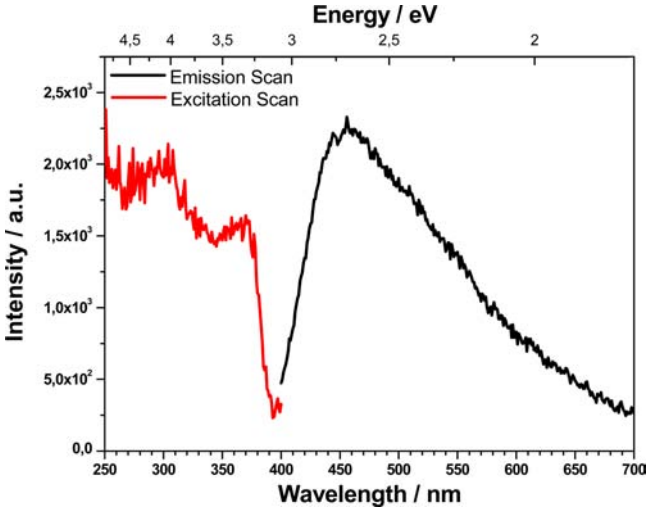

Figure 10. Excitation and emission spectrum of $RbGd[Si(CN_2)_4]$ (emission spectrum upon 360 nm excitation; excitation spectrum monitored for the emission peak at 466 nm).

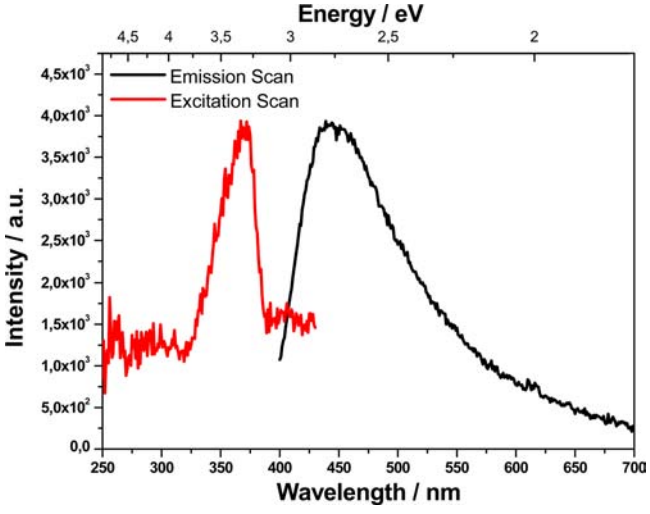

Figure 11. Excitation and emission spectrum of $RbGd[Ge(CN_2)_4]$ (emission spectrum upon 370 nm excitation; excitation spectrum monitored for the emission peak at 460 nm).

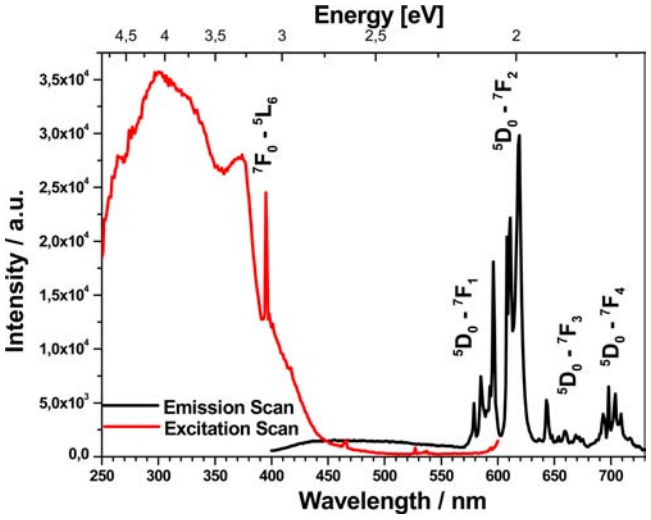

Figure 12. Excitation and emission spectrum of $RbGd[Si(CN_2)_4]:Eu^{3+}$ (emission spectrum upon 375 nm excitation; excitation spectrum monitored for the emission peak at 619 nm).

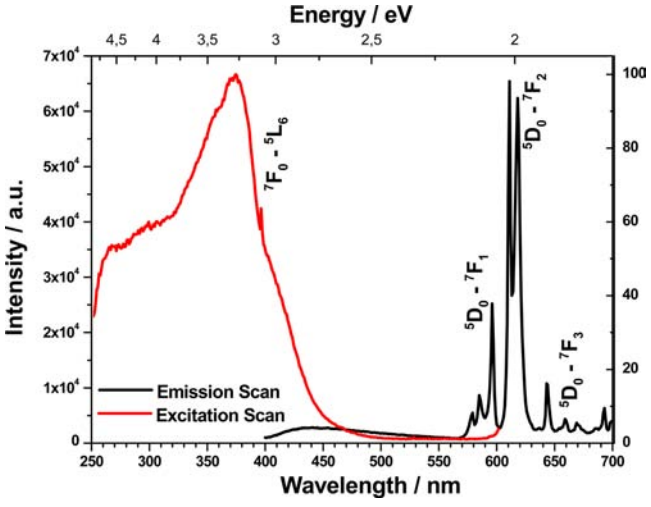

Figure 13. Excitation and emission spectrum of $RbGd[Ge(CN_2)_4]:Eu^{3+}$ (emission spectrum upon 375 nm excitation; excitation spectrum monitored for the emission peak at 618 nm).

$^5D_0 \rightarrow {}^7F_2$ is an electric dipole transition,[33] which requires a lack of inversion symmetry onto the respective Eu^{3+} sites. The intensity of different $[Xe]4f^6 \rightarrow [Xe]4f^6$ transitions of Eu^{3+} depends on the local environment of europium ion. The offset of the emission wavelengths of the two doped host materials are less than 1 nm. Both compounds thus offer a similar environment for the Eu^{3+} ion.

Figures 14 and 15 depict the luminescence and reflection spectra of the Ce^{3+} doped samples. The emission spectra (excited under 356 and 380 nm) show a small red shift of a few nanometers from $RbGd[Si(CN_2)_4]:Ce^{3+}$ to $RbGd[Ge(CN_2)_4]:Ce^{3+}$. In contrast to that, the excitation spectrum, which was monitored for the emission band at 465 nm, shows a strong shift. $RbGd[Si(CN_2)_4]:Ce^{3+}$ shows excitation bands at 288 nm ($^2F_{5/2} \rightarrow {}^2D_{5/2}$) and 356 nm ($^2F_{5/2} \rightarrow {}^2D_{3/2}$). The splitting of the excitation bands is 6700 cm^{-1}. $RbGd[Ge(CN_2)_4]:Ce^{3+}$ shows the excitation bands at 277 and 397 nm corresponds to an excitation band splitting of 10 900 cm^{-1}. The strong dependence for the Ce^{3+} doped compounds is caused by the fact that the respective Ce^{3+} luminescence is due to a interconfigurational $[Xe]4f^1 \rightarrow [Xe]5d^1$ transition in contrast to the luminescence of Eu^{3+} and Tb^{3+}, which exhibit mainly intraconfigurational transitions.

Finally, Figures 16 and 17 exhibit excitation and emission spectra of $RbGd[Si(CN_2)_4]:Tb^{3+}$ and $RbGd[Ge(CN_2)_4]:Tb^{3+}$. Both excitation spectra were monitored for the $^5D_4 \rightarrow {}^7F_5$ transition of Tb^{3+} located at 544 nm and show the band gap excitation at 380 nm and a strong absorption peak at about 275 nm, which is caused by a $^7F_6 \rightarrow {}^5I_J$ transition of Tb^{3+}. The emission spectra under 375 and 379 nm excitation for $RbGd[Si(CN_2)_4]:Tb^{3+}$ and $RbGd[Ge(CN_2)_4]:Tb^{3+}$, respectively, show four strong emission line multiplets due to the transitions $^5D_4 \rightarrow {}^7F_6$ (≈486 nm), $^5D_4 \rightarrow {}^7F_5$ (≈544 nm), $^5D_4 \rightarrow {}^7F_4$ (≈582 nm), and $^5D_4 \rightarrow {}^7F_3$ (≈620 nm). It is not surprising that the emission spectrum of both Tb^{3+} activated materials does not show any differences, because the crystallographic site, onto which Tb^{3+} is incorporated, is very similar in both compounds.

dx.doi.org/10.1021/ic401201w | Inorg. Chem. 2013, 52, 12372−12382

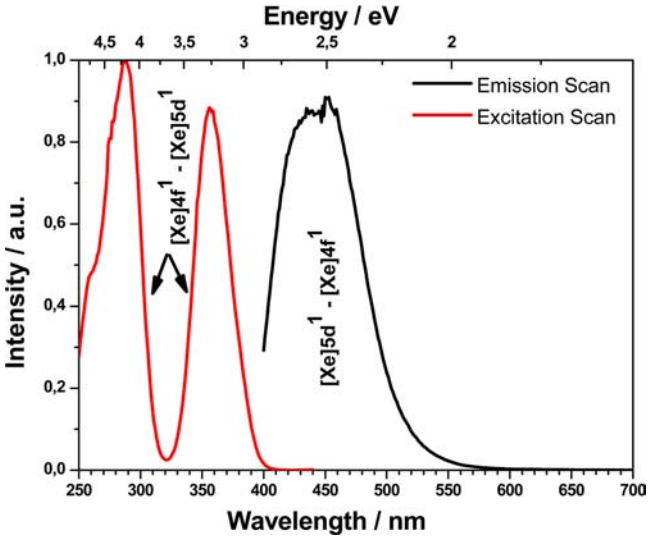

Figure 14. Excitation and emission spectrum of RbGd[Si-$(CN_2)_4$]:Ce^{3+} (emission spectrum upon 356 nm excitation; excitation spectrum monitored for the emission peak at 465 nm).

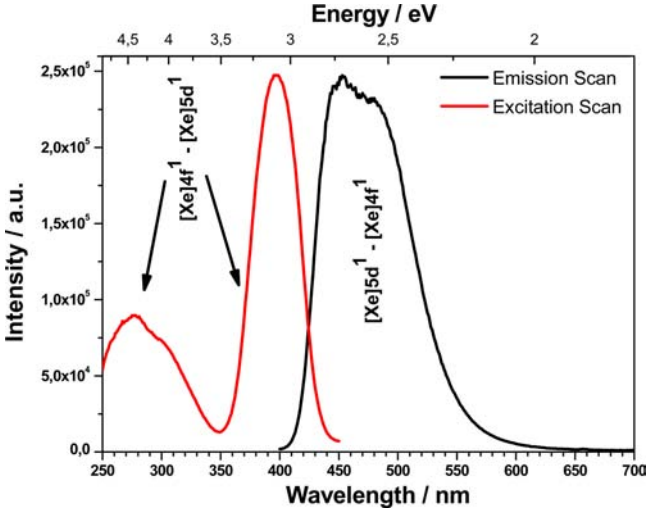

Figure 15. Excitation and emission spectrum of RbGd[Ge-$(CN_2)_4$]:Ce^{3+} (emission spectrum upon 380 nm excitation; excitation spectrum monitored for the emission peak at 465 nm).

Infrared Spectroscopy. Infrared spectra of RbLa[Si-$(CN_2)_4$] and RbLa[Ge$(CN_2)_4$] were measured between 4000 and 400 cm^{-1}. The characteristic vibration frequencies for δ(M−N) (587 cm^{-1} for Si−N and 527 cm^{-1} for Ge−N) as well as 2δ(M−N) (774 cm^{-1} for Si−N and 718 cm^{-1} for Ge−N) match with values found in other tetrahedral coordinated silicon and germanium compounds quite well.[14] Asymmetric stretching vibrations for Si−N and Ge−N were found at 2069 and 2036 cm^{-1}.[36] The lower vibration frequencies found for the Ge−N deformation can be explained with the heavier tetrel and a weaker Ge−N bond.

Bending vibrations of $[NCN]^{2-}$ ions in RbLa[Si$(CN_2)_4$] and RbLa[Ge$(CN_2)_4$] were found at 602 and 600 cm^{-1}, symmetric stretching vibrations at 1287 and 1259 cm^{-1}, and asymmetric stretching vibrations at 2124 and 2107 cm^{-1}, respectively.[12,37] All combinations are found at corresponding wave numbers. An overview of all vibration bands in the recorded spectra is shown in Table 3.

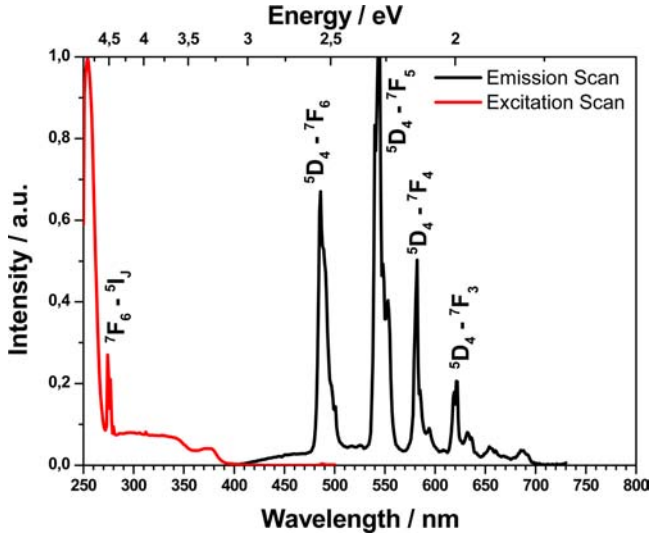

Figure 16. Excitation and emission spectrum of RbGd[Si-$(CN_2)_4$]:Tb^{3+} (emission spectrum upon 370 nm excitation; excitation spectrum monitored for the emission peak at 544 nm).

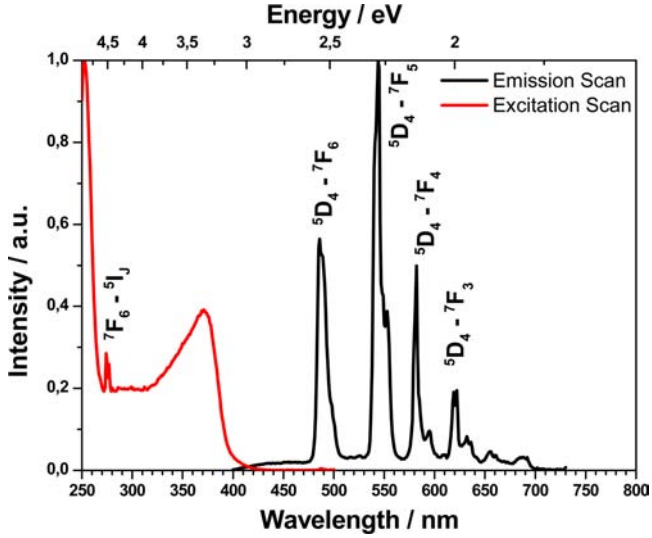

Figure 17. Excitation and emission spectrum of RbGd[Ge-$(CN_2)_4$]:Tb^{3+} (emission spectrum upon 370 nm excitation; excitation spectrum monitored for the emission peak at 544 nm).

Table 3. Vibrational Frequencies for RbLa[$T(CN_2)_4$] (T = Si, Ge) in cm^{-1} [12,36,37]

RbLa[Si$(CN_2)_4$]	RbLa[Ge$(CN_2)_4$]
δ (Si−N) = 587, 774	δ (Ge−N) = 527, 718
2δ (Si−N) = 1209, 1496	2δ (Ge−N) = 1005, 1492
ν_{as} (Si−N) = 2069	ν_{as} (Ge−N) = 2036
δ (N−C−N) = 602	δ (N−C−N) = 600
2δ (N−C−N) = 1198	2δ (N−C−N) = 1190
ν_s (N−C−N) = 1287	ν_s (N−C−N) = 1259
ν_{as} (N−C−N) = 2124	ν_{as} (N−C−N) = 2107
ν_{as} + ν_s (N−C−N) = 3410	ν_{as} + ν_s (N−C−N) = 3350
1357 (w), 1664 (w), 2600 (w)	1373 (w), 1633 (w), 2529 (w)

CONCLUSION

The synthesis of complex solid state compounds with the $[T(CN_2)_4]^{4-}$ anion (T = Si and Ge) was established, and their

dx.doi.org/10.1021/ic401201w | Inorg. Chem. 2013, 52, 12372−12382

formation conditions were monitored and interpreted by thermal analyses. It is shown that their formation reactions by solid state metathesis have ignition temperatures near 400 °C. The structure and identity of $RbRE[Ge(CN_2)_4]$ compounds were elucidated by the combination of X-ray powder diffraction, multinuclear solid state NMR spectroscopy, and DFT calculations.

A homologous series $ARE[Ge(CN_2)_4]$ compounds can be regarded to exist with various combinations of rare earth and alkali metals. All compounds observed so far have been shown to behave stable in air and water. A continuation of this research will be challenging in order to explore more complex solid state compounds of this type, which have no known counterparts in the field of solution chemistry. The successful employment of a useful flux medium can be a key feature for preparations by means of SSM.

The optical reflection spectra of these compounds revealed that the band edge is at about 3.3 eV, which is a suitable value to act as hosts for RE activated luminescent materials. It turned out that Ce^{3+}, Eu^{3+}, or Tb^{3+} doped $RbRE[Ge(CN_2)_4]$ samples show efficient photoluminescence with an emission spectrum typical for the respective RE activator. The energetic position of the lowest crystal-field component of the 4f5d configuration (Ce^{3+} and Tb^{3+}) as well as of the charge-transfer band of Eu^{3+} enables these materials to work as photoluminescent converters, excitable in the UVA range. These findings justify a closer look onto this class of compounds as promising hosts for phosphors (e.g., applicable in near UV emitting LEDs).

■ ASSOCIATED CONTENT

Supporting Information

^{87}Rb and ^{139}La experimental and calculated NMR spectra and ^{29}Si MAS NMR spectrum of $RbLa[Si(CN_2)_4]$ recorded at 14.1 T. This material is available free of charge via the Internet at http://pubs.acs.org.

■ AUTHOR INFORMATION

Notes

The authors declare no competing financial interest.

■ ACKNOWLEDGMENTS

Support of this research by the Deutsche Forschungsgemeinschaft (Bonn) through the project Solid State Metathesis Reactions (ME:25-1) is gratefully acknowledged from scientists of the Eberhard Karls University in Tübingen. M.K. is indebted to the Landesgraduiertenförderung of the Science Ministry of Baden-Württemberg (Universität Tübingen) for supporting his work with a fellowship. S.K. is grateful to the Natural Sciences and Engineering Research Council (NSERC) of Canada and the Canada Foundation for Innovation (CFI) for operating and infrastructure support, respectively. Access to the 900 MHz NMR spectrometer and CASTEP software was provided by the National Ultrahigh-Field NMR Facility for Solids (Ottawa, Canada), a national research facility funded by the Canada Foundation for Innovation, the Ontario Innovation Trust, Recherche Québec, the National Research Council Canada, and Bruker BioSpin and managed by the University of Ottawa (www.nmr900.ca). NSERC is acknowledged for a Major Resources Support grant.

■ REFERENCES

(1) (a) Srinivasan, R.; Ströbele, M.; Meyer, H.-J. *Inorg. Chem.* **2003**, *42*, 3406−3411. (b) Srinivasan, R.; Glaser, J.; Tragl, S.; Meyer, H.-J. *Z. Anorg. Allg. Chem.* **2005**, *631*, 479−483. (c) Sindlinger, J.; Glaser, J.; Bettentrup, H.; Jüstel, T.; Meyer, H.-J. *Z. Anorg. Allg. Chem.* **2007**, *633*, 1686−1690. (d) Glaser, J.; Unverfehrt, L.; Bettentrup, H.; Heymann, G.; Huppertz, H.; Jüstel, T.; Meyer, H.-J. *Inorg. Chem.* **2008**, *47*, 10455−10460.

(2) (a) Gibson, K.; Ströbele, M.; Blaschkowski, B.; Glaser, J.; Weisser, M.; Srinivasan, R.; Kolb, H.-J.; Meyer, H.-J. *Z. Anorg. Allg. Chem.* **2003**, *629*, 1863−1870. (b) Unverfehrt, L.; Glaser, J.; Ströbele, M.; Tragl, S.; Gibson, K.; Meyer, H.-J. *Z. Anorg. Allg. Chem.* **2009**, *635*, 479−483.

(3) Neukirch, M.; Tragl, S.; Meyer, H.-J. *Inorg. Chem.* **2006**, *45*, 8188−8193.

(4) Glaser, J.; Meyer, H.-J. *Angew. Chem., Int. Ed.* **2008**, *47*, 7547−7550.

(5) Glaser, J.; Bettentrup, H.; Jüstel, T.; Meyer, H.-J. *Inorg. Chem.* **2010**, *49*, 2954−2959.

(6) Unverfehrt, L.; Kalmutzki, M.; Ströbele, M.; Meyer, H.-J. *Dalton Trans.* **2011**, *40*, 9921−9924.

(7) Seifer, G. B. *Russ. J. Coord. Chem.* **2002**, *28*, 301−324.

(8) Blaschkowski, B.; Jing, H.; Meyer, H.-J. *Angew. Chem., Int. Ed.* **2002**, *41*, 3322−3336.

(9) Unverfehrt, L.; Ströbele, M.; Glaser, J.; Meyer, H.-J. *Z. Anorg. Allg. Chem.* **2009**, *635*, 1947−1952.

(10) Kalmutzki, M.; Ströbele, M.; Meyer, H.-J. *Dalton Trans.* **2013**, *42*, 12934−12939.

(11) Jing, H. *Dissertation*, Universität Tübingen, Tübingen, Germany, 2002.

(12) Unverfehrt, L.; Kalmutzki, M.; Ströbele, M.; Meyer, H.-J. *Dalton Trans.* **2011**, *40*, 9921−9924.

(13) Unverfehrt, L. *Dissertation*, Universität Tübingen, Tübingen, Germany, 2011.

(14) (a) Dahrouch, M.; Rivière-Baudet, M.; Katir, N.; Alvarez, J.; Diaz, E.; Rivière, P.; Castel, A.; Chavez, I.; Manriquez, J. M. *Inorg. Chim. Acta* **2007**, *360*, 4031−4036. (b) Riedel, R.; Kroke, E.; Greiner, A.; Gabriel, A. O.; Ruwisch, L.; Nicolich. *J. Chem. Mater.* **1998**, *10*, 2964−2979.

(15) Winkler, H.; Benker, A.; Petry, R., Vosgroene, T. Int. Patent: WO 2012/010243, January 26, 2012.

(16) Meyer, G.; Ax, P. *Mater. Res. Bull.* **1982**, *17*, 1447−1455.

(17) Eichele, K.; Wasylishen, R. E. *WSOLIDS1 NMR simulation package*, Version 1.17.30, Dalhousie University, Halifax, Canada and University of Tübingen, Tübingen, Germany, 2001.

(18) Clark, S. J.; Segall, M. D.; Pickard, C. J.; Hasnip, P. J.; Probert, M. J.; Refson, K.; Payne, M. C. *Z. Kristallogr.* **2005**, *220*, 567−570.

(19) (a) Wu, G.; Zhu, J. *Prog. Nucl. Mag. Res. Spectrosc.* **2012**, *61*, 1−70. (b) Willans, M. J.; Feindel, K. W.; Ooms, K. J.; Wasylishen, R. E. *Chem.—Eur. J.* **2006**, *12*, 159−168.

(20) Zemczuzny, S.; Rambach, F. *Z. Anorg. Allg. Chem.* **1910**, *65*, 403−428.

(21) *WinXPOW*, Version 1.10: Diffractometer Software; Stoe&Cie GmbH, Darmstadt, Germany, 2001.

(22) Gruen, R. *Acta Crystallogr.* **1979**, *35*, 800−804.

(23) Wild, S.; Grieveson, P.; Jack, K. H. *Spec. Ceram.* **1972**, *5*, 385−393.

(24) Michaelis, V. K.; Kroeker, S. *J. Phys. Chem. C* **2010**, *114*, 21736−21744.

(25) Greer, B. J.; Michaelis, V. K.; Terskikh, V. V.; Kroeker, S. *Can. J. Chem.* **2011**, *89*, 1118−1129.

(26) Sutrisno, A.; Hanson, M. A.; Rupar, P. A.; Terskikh, V. V.; Baines, K. M.; Huang, Y. *Chem. Commun.* **2010**, *46*, 2817−2819.

(27) Hanson, M. A.; Sutrisno, A.; Terskikh, V. V.; Baines, K. M.; Huang, Y. *Chem.—Eur. J.* **2012**, *18*, 13770−13779.

(28) MacKenzie, K. J. D.; Smith, M. E. *Multinuclear Solid-State NMR of Inorganic Materials*; Pergamon: New York, 2002.

(29) Michaelis, V. K.; Aguiar, P. M.; Kroeker, S. *J. Non-Cryst. Solids* **2007**, *353*, 2582−2590.

(30) Hamaed, H.; Lo, A. Y. H.; Lee, D. S.; Evans, W. J.; Schurko, R. W. *J. Am. Chem. Soc.* **2006**, *128*, 12638−12639.
(31) Rollet, A.-L.; Allix, M.; Veron, E.; Deschamps, M.; Montouillout, V.; Suchomel, M. R.; Suard, E.; Barre, M.; Ocana, M.; Sadoc, A.; Boucher, F.; Bessada, C.; Massiot, D.; Fayon, F. *Inorg. Chem.* **2012**, *51*, 2272−2282.
(32) Spencer, L.; Coomes, E.; Ye, E.; Terskikh, V. V.; Ramzy, A.; Thangadurai, V.; Goward, G. R. *Can. J. Chem.* **2011**, *89*, 1105−1117.
(33) Sekine, T.; Tansho, M.; Kanzaki, M. *Appl. Phys. Lett.* **2001**, *78*, 3050−3051.
(34) Harris, R. K.; Olivieri, A. C. *Prog. Nuc. Magn. Res. Spectrosc.* **1992**, *24*, 435−456.
(35) (a) Blasse, G.; Grabmaier, B. C. *Luminescent Materials*; Springer-Verlag: Berlin, 1994. (b) *Phosphor handbook*, 2nd ed.; Yen, W. M., Shionoya, S., Yamamoto, H., Eds.; The CRC Press laser and optical science and technology series; CRC Press/Taylor and Francis: Boca Raton, FL, 2007.
(36) (a) Weidlein, J.; Müller, U.; Dehnicke, K. *Schwingungsfrequenzen I*; Georg Thieme Verlag: Stuttgart-New York, 1981. (b) Weidlein, J.; Müller, U.; Dehnicke, K. *Spektroskopie*; Georg Thieme Verlag: Stuttgart-New York, 1982.
(37) (a) Berger, U.; Schnick, W. *J. Alloys Compd.* **1994**, *206*, 179−184. (b) Becker, M.; Nuss, J.; Jansen, M. *Z. Anorg. Allg. Chem.* **2000**, *626*, 2505−2508. (c) Schnick, W.; Huppertz, H. *Z. Anorg. Allg. Chem.* **1995**, *621*, 1703−1707. (d) Harper, A.; Hubberstey, P. *J. Chem. Res. (S)* **1989**, *7*, 194−195. (e) Reckeweg, O.; DiSalvo, F. J. *Z. Anorg. Allg. Chem.* **2003**, *629*, 177−179. (f) Lui, X.; Müller, P.; Knoll, P.; Dronskowski, R. *Inorg. Chem.* **2002**, *41*, 4259−4265. (g) Becker, M.; Nuss, J.; Jansen, M. *Z. Naturforsch., B: J. Chem. Sci.* **2000**, *55b*, 383−385. (h) Down, M. G.; Haley, M. J.; Hubberstey, P.; Pulham, R. J.; Thunder, A. E. *J. Chem. Soc., Dalton Trans.* **1978**, *10*, 1407−1411.